Synthesis of Todorokite at Atmospheric Pressure

Xiong Han Feng,[†] Wen Feng Tan,[†] Fan Liu,*[,†] Jian Bo Wang,[‡] and Huada Daniel Ruan[§]

College of Resources & Environment, Huazhong Agricultural University, Wuhan 430070, People's Republic of China, Department of Physics and Center for Electron Microscopy, Wuhan University, Wuhan 430072, People's Republic of China, and Alpine Green Technology Consultants, Ltd., 12th Floor, China Trade Centre, 122-124 Wai Yip Street, Kwun Tong, Kowloon, Hong Kong

Received January 7, 2004. Revised Manuscript Received August 15, 2004

A 3 × 3 tunnel-structured manganese oxide, todorokite, or MnO_6 octahedral molecular sieve (OMS-1), was synthesized at atmospheric pressure by a refluxing process from birnessite, the layer-structured precursor. The todorokite synthesized by the refluxing process (named as OMS-1-R) consisted of fibers with various lengths and platy trilling patterns, made of fiber crystals twinned with each other at 120°, from which the fibers matted and extended. Intergrowth of different widths of tunnels commonly occurred in a disorderly manner, with a triple octahedral chain width being the most predominant. Such morphological and intergrowth characteristics were similar to those of natural todorokites and a hydrothermally synthesized todorokite. When refluxing time was increased, the crystallinity of OMS-1-R was promoted and small scale twinning in morphology became a relatively large and coarse twinning. However, there was no other crystalline phase produced. The OMS-1-R24, synthesized after 24 h of refluxing, with a chemical composition of $Mg_{0.17}MnO_{2.10}(H_2O)_{0.88}$, was stable up to 400 °C. The BET surface area was found to be 77 m^2/g, and the surface was predominantly mesoporous with the BJH adsorption average pore diameter of 14 nm.

Introduction

Todorokites are a family of large tunnel-structured manganese oxides with a 3 × 3 array of edge-shared MnO_6 octahedra, commonly found in terrestrial manganese ore deposits, weathering products of rocks rich with manganese, and marine manganese nodules.[1−3] They have a stable microporous molecular sieve structure similar to that of zeolite.[4] As an important component of nodules, todorokites are good hosts for the accumulation of many transition metals in marine environments, such as Cu, Ni, and Co.[5] In addition, both Lewis and Brönsted sites on the surface and a high redox potential offer todorokites preferable catalyst activity and selectivity in a variety of industrially important reactions.[4] The large tunnel dimension of todorokites may allow faster intercalation and deintercalation of Li^+ with excellent electrochemical reversibility and stability.[6] In addition to being a potential polymetallic resource,[7] promising applications for todorokite include their use as adsorbents, heterogeneous catalysts and molecular sieves, sensors, and rechargeable battery material.[4−10]

Natural todorokites typically occur as poorly crystallized nanometer particles mixed with many other minerals. Low content and poor crystallinity make fundamental studies and their direct industrial application very difficult. Synthesis of todorokite is a promising alternative. Under hydrothermal conditions, todorokite was first synthesized by Golden et al. through autoclave treatment of Mg^{2+} exchanged birnessite (Mg-buserite) at 155 °C.[9] Suib and co-workers developed oxidation of $Mn(OH)_2$ with $Mg(MnO_4)_2$ to prepare birnessite in alkali media, and subsequently obtained another thermally stable version of todorokite by autoclave treatment of Mg-buserite from 155 to 170 °C.[4] Other methods to synthesize todorokite, using different procedures of birnessite preparation or modes of heating during todorokite formation, have also been reported.[11−14] However, hydrothermal treatment of large metal ions exchanged birnessite in autoclave at a relative high

* To whom correspondence should be addressed.
[†] Huazhong Agricultural University.
[‡] Wuhan University.
[§] Alpine Green Technology Consultants, Ltd.

(1) Turner, S.; Siegel, M. D.; Buseck, P. R. *Nature* **1982**, *296*, 841−842.
(2) Post, J. E. *Proc. Natl. Acad. Sci. U.S.A.* **1999**, *96*, 3447−3454.
(3) Siegel, M. D.; Turner, S. *Science* **1983**, *219*, 172−174.
(4) Shen, Y. F.; Zerger, R. P.; Suib, S. L.; McCurdy, L.; Potter, D. I.; O'Yang, C. L. *Science* **1993**, *260*, 511−515.
(5) Mellin, T. A.; Lei, G. *Mar. Geol.* **1993**, *115*, 67−83.
(6) Duncan, M. J.; Leroux, F.; Corbett, J. M.; Nazar, L. F. *J. Electrochem. Soc.* **1998**, *145*, 3746−3757.
(7) Burns, R. G.; Burns, V. M.; Stockman, H. W. *Am. Mineral.* **1985**, *70*, 205−208.
(8) Dyer, A.; Pillinger, M.; Newton, J.; Harjula, R.; Moller, T.; Amin, S. *Chem. Mater.* **2000**, *12*, 3798−3804.
(9) Tian, Z. R.; Yin, Y. G.; Suib, S. L. *Chem. Mater.* **1997**, *9*, 1126−1133.
(10) Suib, S. L. *Chem. Innov.* **2000**, *30*, 27−33.
(11) Golden, D. C.; Chen, C. C.; Dixon, J. B. *Science* **1986**, *231*, 717−719.
(12) Ching, S.; Krukowska, K. S.; Suib, S. L. *Inorg. Chim. Acta* **1999**, *294*, 123−132.
(13) Vileno, E.; Ma, Y.; Zhou, H.; Suib, S. L. *Microporous Mesoporous Mater.* **1998**, *20*, 3−15.
(14) Feng, Q.; Yanagisawa, K.; Yamasaki, N. *J. Porous Mater.* **1998**, *5*, 153−161.

10.1021/cm0499545 CCC: $27.50
Published on Web 10/01/2004

temperature and pressure is the unique procedure of todorokite synthesis. Low productivity, difficulties in controlling the reaction, and the high costs of hydrothermal synthesis in a limited autoclave container obstruct the further profound studies and extensive applications of todorokite.

In this work, a refluxing process at atmospheric pressure was developed to prepare large amounts of thermally stable todorokites. Transformation of Mg-buserite to todorokite was monitored by X-ray diffraction (XRD). Infrared spectroscopy (IR), Raman spectroscopy (RS), transmission electron microscopy (TEM), high-resolution transmission electron microscopy (HRTEM), nitrogen sorptometry, and thermogravimetric analysis (TGA) techniques were used to characterize the synthetic todorokites.

Experimental Section

Synthesis Procedure. The synthesis of todorokite included two steps. First, birnessite was prepared in alkali media under vigorous stirring at room temperature, as reported in our previous work[15] (see Supporting Information). The purified birnessite had a chemical composition of $Na_{0.25}MnO_{2.07}\cdot 0.66H_2O$ with an average oxidation state (AOS) of 3.89. The results of X-ray diffraction (XRD), infrared (IR) spectroscopy, and electron microscopy analysis have already confirmed that the birnessite was a pure crystalline phase.[15] About 10 g of purified birnessite, which remained in the wet state, was then dispersed in 2 L of 1 mol/L $MgCl_2$ solution. After being fully exchanged for 12 h under the condition of continuous shaking, Mg-buserite was obtained by centrifuging and washing. The Mg-buserite was dispersed in 300 mL of distilled deionized water in a 500 mL triangle beaker connected with a condensation device and heated to reflux under stirring. After being refluxed for 8−24 h, the suspension was cooled to room temperature, washed until the conductivity of the supernatant was below 2.0 μS/cm, and freeze-dried.

Characterization. X-ray powder diffraction was carried out at ambient temperature, using a D/Max-3B diffractometer equipped with a monochromated Fe Kα radiation ($\lambda = 0.19373$ nm). The diffractometer was operated at a tube voltage of 40 kV and a tube current of 20 mA. Both Mg-buserite and todorokite have a basal *d* spacing of 1 nm. Mg-buserite is not stable and can be transformed to the 0.7 nm phase (birnessite) when heating or dehydrating. However, todorokite has a relatively high thermal stability.[16] For the identification of todorokite, before XRD analysis the oriented slides for the intermediate products were heated for 12 h at 140 °C to eliminate the interference of diffraction peaks of Mg-buserite. As such, the 1 nm peak in the diffraction pattern could be attributable to the characteristic peak of todorokite. Meanwhile, powder XRD analysis of random orientation was performed for the characterization of the final todorokite products without heating. The reference of α-SiO_2 was used as a standard in crystal size analysis.

Transmission IR spectra were obtained with a Bruker Equinox 55 model spectrophotometer by making pellets with KBr. The resolution was set at 4 cm^{-1} with a scan number of 15. The Raman scattering spectra were taken at room temperature in reflection geometry using a Renishaw RM-1000 micro-Raman system. The excitation source was a 514.5 nm line from a model 160-series Argon-ion Laser System. To avoid sample photo transformation, Raman spectra were recorded using a low excitation power of 10 mW[17] and 75% of the excitation power was filtered before the laser beam reached the samples. The samples were pressed gently as a pellet form for Raman analysis. Transmission electron microscopy analysis was carried out with a Philips-CM12 TEM operated at 120 kV. The sample was gently crushed to powder, and then dispersed in absolute alcohol and sonicated prior to deposition on a holey carbon film. The HRTEM was performed on sample suspensions dried on a holey carbon grid with a JEOL JEM 2010 FEF electron microscope operated at 200 kV.

The TGA was carried out on a NETZSCH STA 449C thermal analysis system using 10 mg of sample powder, in a dynamic air current at a flow rate of 20 mL/min with a heating rate of 10 °C/min. Nitrogen sorptometry was measured at liquid nitrogen temperature (−195 °C), using an automatic ASAP 2010 Micromeritics sorptometer equipped with an outgassing platform and on-line data acquisition and handling system operating standard BET,[18] *t*,[19] and BJH[20] analytical software for the adsorption data. Before being exposed to the nitrogen atmosphere, 300 mg of sample was evacuated at 100 °C and 10^{-5} Torr for 12 h.

For the determination of elemental composition, 150 mg of sample was dissolved in 50 mL of aqua regia and diluted to 1000 mL. The contents of Na, Mn, and Mg were analyzed by a Varian Vista-MPX ICP-OES. The average oxidation state (AOS) of Mn was measured by the oxalic acid-permanganate back-titration method.[21] Briefly, 0.1 g of the sample was completely dissolved in 10 mL of 0.5 M $H_2C_2O_4$ and 10 mL of 0.5 M H_2SO_4 to reduce all of the manganese to Mn^{2+}. The extra $C_2O_4^{2-}$ was determined by back-titration at 60 °C with standardized 0.02 M $KMnO_4$ solution. The AOS of Mn was calculated on the basis of both the titration result and the total amount of Mn determined by ICP. The water percentage was calculated from the weight difference.

Results and Discussion

Synthesis of Todorokites. To understand the formation of todorokite from birnessite under the refluxing process, XRD analyses on the intermediate and final products were conducted in the synthesis. The nomenclature for the synthetic todorokites is as follows: OMS-1-R8 and OMS-1-R24 represent synthesized todorokite (OMS-1) by the refluxing processing (R) for 8 h (8) and 24 h (24), respectively.

Transformation Process. The XRD patterns in Figure 1 showed the phases of the intermediate products at the different stages of refluxing process. A very weak 1 nm diffraction peak and a strong 0.7 nm peak in the XRD pattern of heat-treated (140 °C) intermediate products obtained after 2 h of reflux indicated that a little part of Mg-buserite had been converted into todorokite. After 6 h of reflux, the intensity of the 1 nm diffraction peak increased, while the intensity of the 0.7 nm peak decreased, suggesting that more todorokite was produced gradually. At a reflux time of 8 h, the 0.7 nm diffraction peak of the product disappeared, and the 1 nm peak became strong. This result showed that Mg-buserite had completely been converted into well-crystallized todorokite after 8 h of refluxing. When the refluxing time was prolonged to 24 h, the characteristic peaks of todorokite in the XRD pattern of the product became stronger, indicating that the crystallinity of the product was further enhanced. No manganite (0.34 nm,

(15) Feng, X. H.; Liu, F.; Tan, W. F.; Liu, X. W. *Clays Clay Miner.* **2004**, *52*, 240−250.
(16) Usui, A.; Mellin, T. A.; Nohara, M.; Yuasa, M. *Mar. Geol.* **1989**, *86*, 41−56.
(17) Julien, C. M.; Massot, M.; Poinsignon, C. *Spectrachim. Acta, Part A* **2004**, *60*, 689−700.
(18) Gregg, S. J.; Sing, K. S. W. *Adsorption, Surface Area and Porosity*; Academic Press: New York, 1967.
(19) Leeloux, A. S. In *Catalysis-Science and Engineering*; Anderson, J. R., Boudart, M., Eds.; Springer-Verlag: Berlin, 1981; pp 171−229.
(20) Barrett, E. P.; Joyner, L. S.; Halenda, P. P. *J. Am. Chem. Soc.* **1951**, *73*, 373−380.
(21) Hem, J. D. *Geochim. Cosmochim. Acta* **1981**, *45*, 1369−1374.

Table 1. Diffraction Data for the Synthetic and Natural Todorokites

OMS-1-R24[a]			natural todorokite (38-475)[b]			natural todorokite (13-164)[c]			hydrothermally synthesized todorokite[d]	
2θ (deg)	d/nm	I/(%)	d/nm	I/(%)	index (hkl)	d/nm	I/(%)	index (hkl)	d/nm	I/(%)
11.56	0.962	100	0.956	100	1 0 0, 0 0 1	0.968	100	1 0 0	0.966	100
15.60	0.714	5	0.706	5	1 0 −1	0.715	2		0.713	5
23.22	0.481	84	0.486	17	2 0 0	0.48	80	0 0 2	0.480	80
25.04	0.447	10	0.446	7	2 0 −1	0.445	5		0.444	10
35.22	0.320	9	0.318	3	0 0 3	0.322	15	0 0 3	0.320	5
45.98	0.248	16	0.245	16	2 1 0	0.246	20	2 1 0	0.248	20
47.38	0.241	38	0.240	36	4 0 −1, 2 1 −1	0.239	40	−2 1 1	0.239	20
48.60	0.235	10	0.235	25	1 1 2	0.234	15	−1 0 4	0.234	10
51.62	0.222	18	0.222	7	2 1 −2	0.222	20		0.223	10
53.54	0.215	3	0.215	2	2 1 2	0.215	5	−2 0 4	0.215	4
58.50	0.198	8	0.199	6	3 1 −2	0.198	20		0.197	5
60.22	0.193	2	0.192	6	3 1 2	0.192	5	0 0 5	0.195	5
67.22	0.174	10	0.174	8	2 1 −4	0.175	10		0.175	10
70.00	0.169	4	0.170	3	4 1 2					
77.92	0.154	3	0.153	5	2 1 −5	0.154	5	−6 0 2	0.154	5
85.82	0.142	10	0.142	16	0 2 0	0.142	30	0 2 0		
87.12	0.140	2	0.141	9	6 1 0, 6 1 −1	0.139	10	7 0 0		

[a] Unheated. [b] From JCPDS 38-475. [c] From JCPDS 13-164. [d] From ref 11.

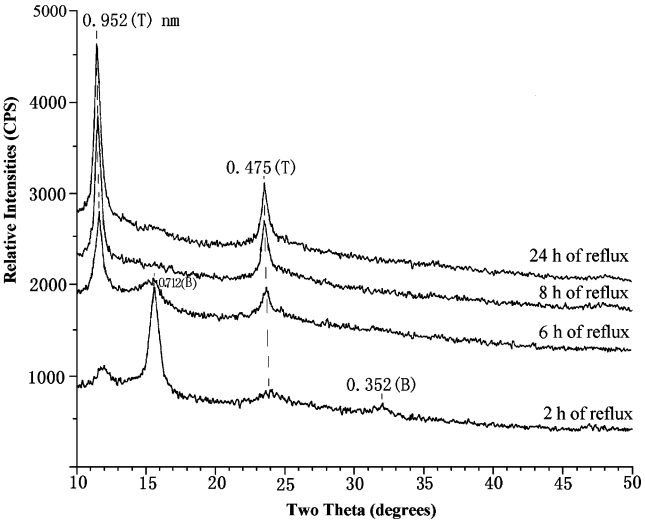

Figure 1. XRD patterns of intermediate products at the different stages of reflux (B, birnessite; T, todorokite) (oriented slide analysis after heating for 12 h at 140 °C).

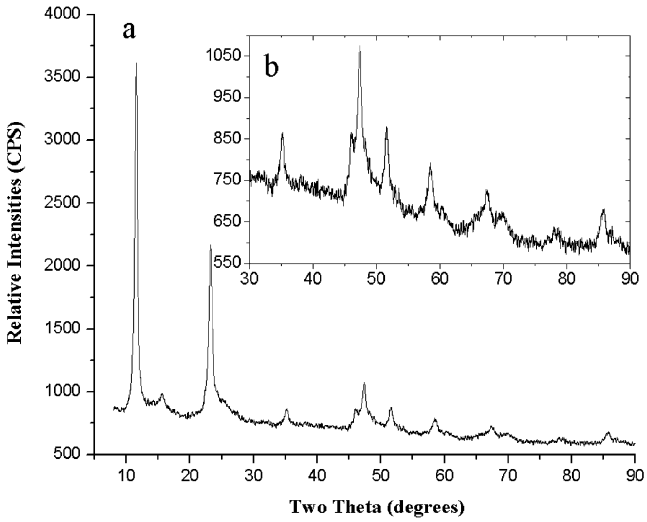

Figure 2. Powder XRD diffraction pattern of OMS-1-R24: (a) 8−90°2θ; (b) 30−90°2θ.

JCPDS 8-99) or other phases were detected from the XRD analysis.

Identification of Todorokite by Powder XRD. The powder XRD pattern (Figure 2) of the synthetic todorokite obtained after refluxing for 24 h provided more detailed diffraction peaks and structure information than those in the oriented XRD pattern (Figure 1). Diffraction data from the synthesized todorokite matched well with those of the naturally formed todorokites (JCPDS 13-164 and JCPDS 38-475) and a synthetic sample from the hydrothermal method (Table 1). The powder XRD analysis further verified the above results, and the 1 nm diffraction peak of the synthetic todorokite was shifted from 0.962 to 0.952 nm due to partial dehydration after heated at 140 °C (Figure 1). As was shown in the powder XRD pattern, the diffraction peaks of the synthetic todorokite were broadened to some extent, especially for the peaks of 0.48 and 0.24 nm, indicating that the crystal size of the synthetic todorokite was small and that significant quantities of tunnels larger than 3 × 3 were probably present in the todorokite.[22] The size of the todorokite crystallite synthesized after 24 h of reflux was 23 nm, calculated using the Scherrer formula[23] from a half peak width of 0.962 nm diffraction peak. The fabric todorokite crystal grows along the b axis, running parallel to the tunnel direction.[22,24] So, from the plane index (1 0 0 or 0 0 1) for the 0.962 nm diffraction peak (Table 1), the calculated crystal particle size was the width or the thickness, that is, the size along the vertical direction of the crystal plane (1 0 0 or 0 0 1), not the length of the fabric crystals.

Characterization of OMS-1-R. *TEM and HRTEM Results.* The morphology of OMS-1-R24 reveals fibers with various lengths, which extend from a platy fiber-matted matrix (Figure 3a). The electron diffraction (ED)

(22) Post, J. E. In *Biomineralization Processes of Iron and Manganese— Modern and Ancient Environments*; Skinner, H. C. W., Fitzpatrick, R. W. Eds.; CATENA Verlag: Cremlingen, 1992; pp 51−73.
(23) Cullity, B. D. *Elements of X-ray Diffraction*, 2nd ed.; Addison-Wesley Publishing Co.: Reading, MA, 1994; pp 99−106.
(24) Golden, D. C.; Chen, C. C.; Dixon, J. B. *Clays Clay Miner.* **1987**, *35*, 271−280.

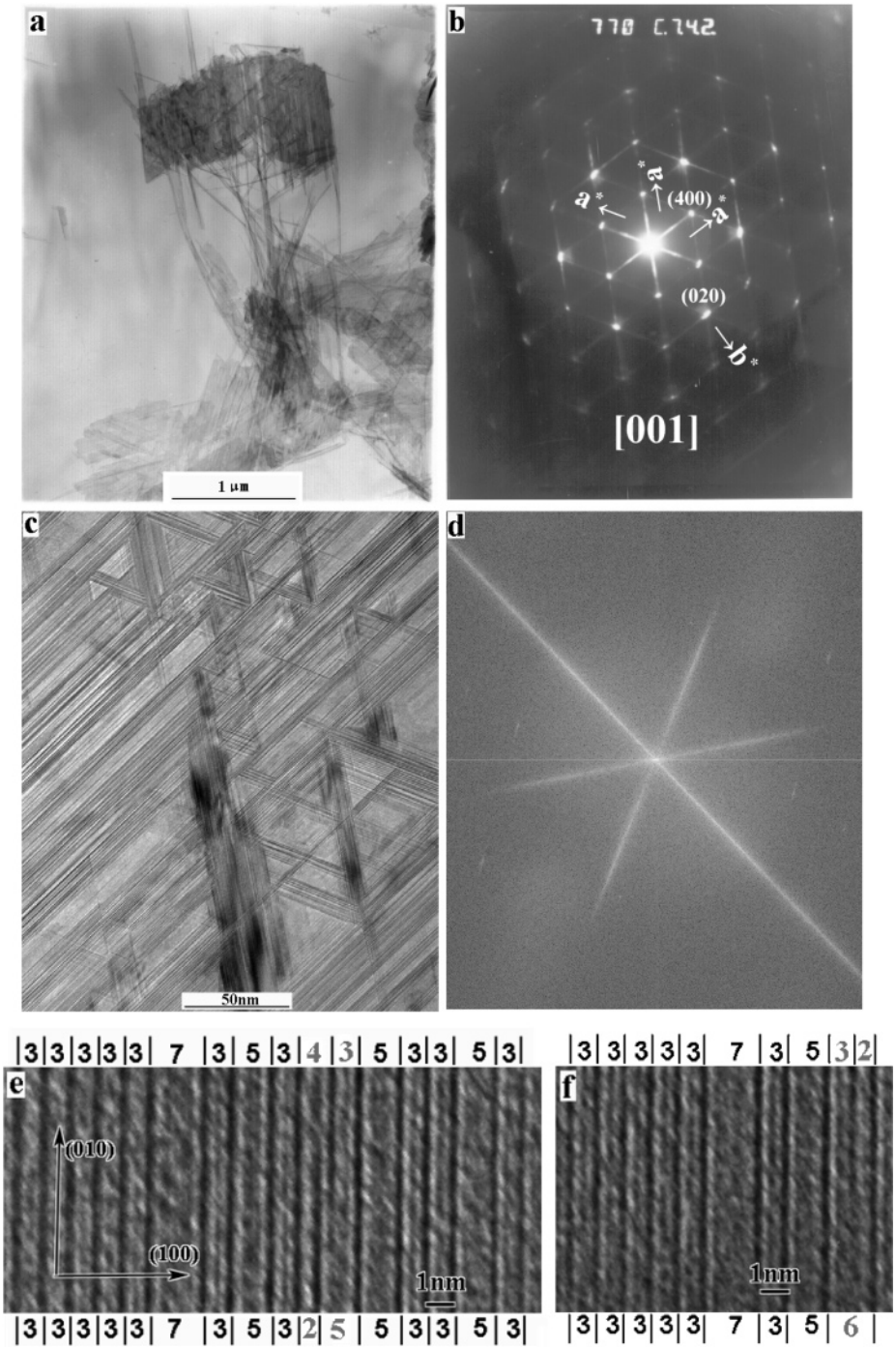

Figure 3. TEM and HRTEM images of OMS-1-R24: (a) TEM image; (b) selected area of electron diffraction of the matted matrix; (c) HRTEM image of the matted matrix; (d) FFT pattern of (c); and (e,f) (001) plane HRTEM images of individual fibers.

pattern of the matrix (Figure 3b) shows a pseudohexagonal symmetry. There were many weak reflection spots close to each other between the strong reflection spots of the (h 0 0) plane to form reflection streakings along three a^* axis directions because of the heterogeneity of the tunnel size,[22,25] or because of the disorder of the tunnel array as a reviewer suggested. The ED patterns were indexed with the reported parameters: space group $P2/m$, $a = 0.976$ nm, $b = 0.284$ nm, $c = 0.956$ nm, and $\beta = 94.16°$.[26] The matrixes observed by HRTEM showed that they were actually trilling patterns formed by fiber crystals twinned with each other at 120° (Figure 3c). The fast Fourier transform (FFT) pattern (Figure 3d) also verified this trilling structure, which was correspondent to the pseudohexagonal symmetry in the ED pattern. With increasing reflux time, the trilling crystal transformed from a small scale into a relatively large and coarse scale (see Supporting Information). From the lattice image of the OMS-1-R across the fiber direction (Figure 3e,f), tunnels of 2, 3, 4, 5, 6, and 7 MnO_6 octahedral chain widths along the a axis could be seen. Among them, the triple chain width (1 nm) was predominant. Intergrowth of different widths of tunnels occurred commonly in a disorderly manner: a 4, 3 chain arranged sequence on the upper

(25) Chukhrov, F. V.; Gorshkov, A. I.; Sivtsov, A. V.; Beresovskaya, V. V. *Nature* **1979**, *278*, 631−632.
(26) Post, J. E.; Bish, D. L. *Am. Mineral.* **1988**, *73*, 861−869.

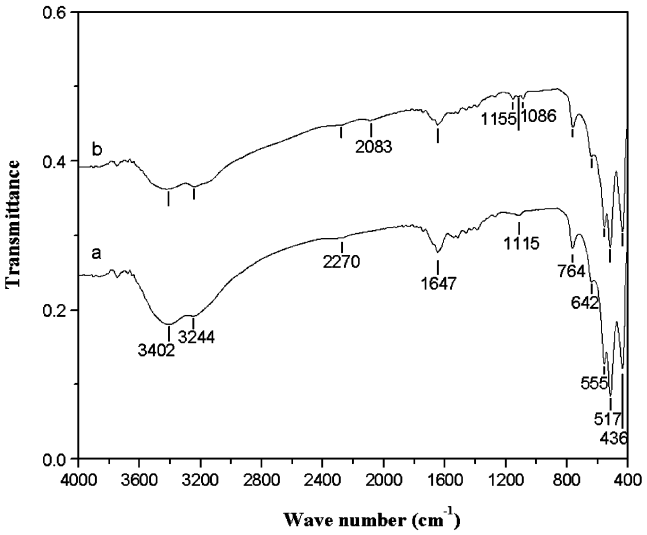

Figure 4. IR spectra of (a) OMS-1-R24 and (b) hydrothermally synthesized todorokite.

side changed to a 2, 5 sequence on the lower side (Figure 3e), and a 3, 2 chain arranged sequence changed to a 6 chain (Figure 3f). Such a morphological and intergrowth nature is the typical characteristic of natural todorokite and can thus be distinguished from other manganese oxides, which can account for the streaking of the ED pattern and the broadening of XRD peaks.[1,11,22,24−26]

IR and RS Results. The IR spectrum of OMS-1-R24 (Figure 4a) was generally in agreement with those of the natural samples[27] and the todorokite synthesized hydrothermally by Golden et al.[11,24] For comparison, hydrothermally synthesized todorokite was obtained by autoclaving the Mg-buserite for 8 h at 155 °C. This product was composed of well-crystallized todorokite without impurity, as determined by XRD. In its IR spectrum (Figure 4b), besides the common bands identical to those of the OMS-1-R24, additional bands appeared at 2083, 1155, and 1086 cm^{-1}, which were identical to the characteristic bands of manganite.[27] The bands near 3200 and 3400 cm^{-1} could be assigned to well-ordered water of strongly hydrogen-bonding and disordered water with a lower degree of hydrogen bonding, respectively.[27,28] It was obvious from Figure 4 that OMS-1-R24 had a stronger band at 3402 cm^{-1} than the hydrothermally synthesized todorokite, indicating that OMS-1-R24 might possess more disordered water in the tunnel than the hydrothermally synthesized todorokite. The Raman spectrum of OMS-1-R24 (Figure 5a) displayed one strong band at 643 cm^{-1} and two weak bands at 357 and 298 cm^{-1}, in good agreement with that of the hydrothermally synthesized todorokite (Figure 5b). However, they were different from those of birnessite (649 cm^{-1}) and Mg-buserite (653 cm^{-1}) (see Supporting Information). The strong Raman band of OMS-1-R24 would be shifted to a high wavenumber after calcination at different temperatures for 2 h, suggesting that OMS-1-R24 might not be altered under laser beam during the recording of the spectra (see Supporting Information). The similarities in IR and Raman spectrum between OMS-1-R and natural todorokites and hydrothermally synthesized samples demonstrated that they were also similar in short-ranged structure. So, OMS-1-R had lattice parameters similar to those of natural todorokites and hydrothermally synthesized samples, as indicated from the XRD data (Table 1).

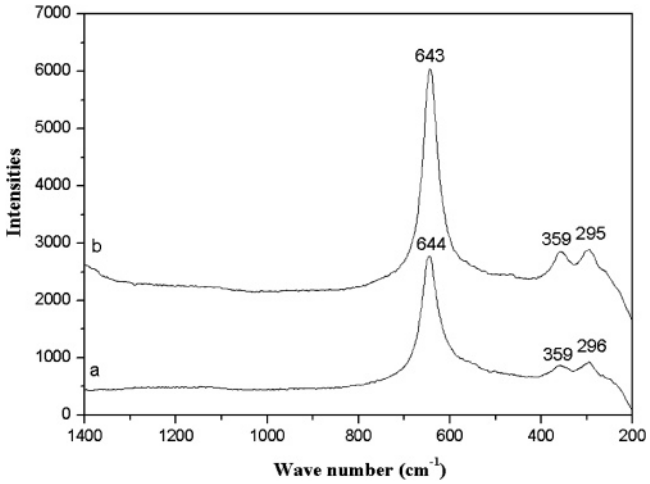

Figure 5. Raman spectra of (a) OMS-1-R24 and (b) hydrothermally synthesized todorokite.

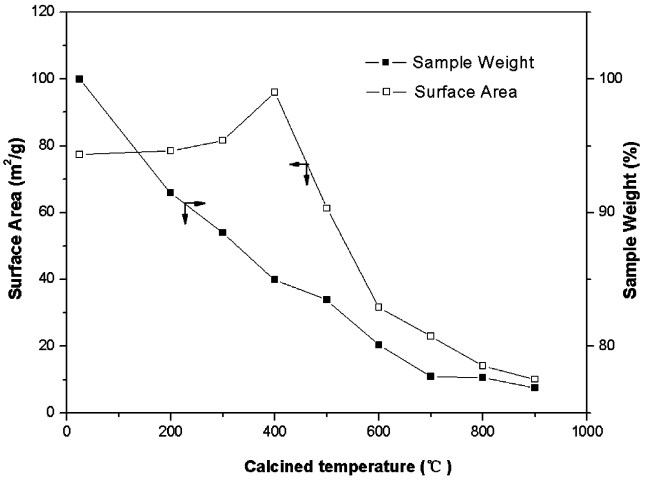

Figure 6. Surface area and weight loss of OMS-1-R24 versus calcined temperature.

Thermal Properties. The XRD analysis for OMS-1-R24 after being calcined for 1 h in the air at different temperatures indicated that todorokite diffraction peaks remained quite strong below 400 °C. At 500 °C, only a weak peak of todorokite at 0.95 nm was detected. Above 600 °C, all of the characteristic peaks of todorokite were gone, but weak peaks of spinel-phases appeared and became stronger with the increase of calcined temperature. Curves of the surface area, measured by the BET method with N_2 as the adsorbate, and weight loss of OMS-1-R24 versus calcined temperature showed that the surface area increased with calcined temperature up to 400 °C and then abruptly decreased (Figure 6). It was reported that the cyclohexane uptake also increased with dehydration temperature in a range and then significantly deceased.[29] The temperature dependence of the surface area resulted from the presence of the

(27) Potter, R. M.; Rossman, G. R. *Am. Mineral.* **1979**, *64*, 1199−1218.

(28) Yang, D. S.; Wang, M. K. *Clays Clay Miner.* **2003**, *51*, 96−101.

(29) Shen, Y. F.; Suib, S. L.; O'Yang, C. L. *J. Am. Chem. Soc.* **1994**, *116*, 11020−11029.

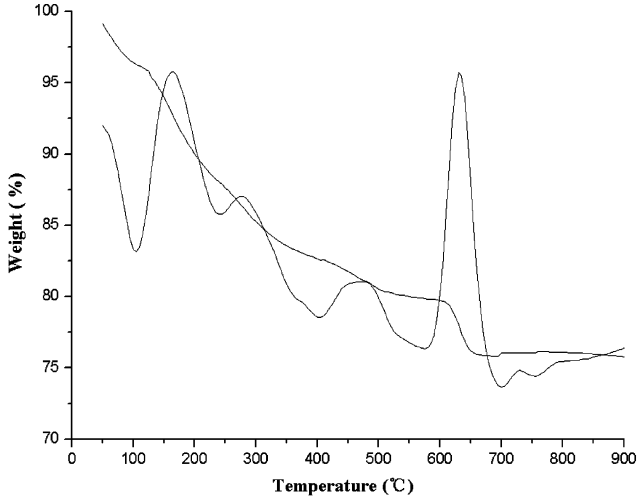

Figure 7. TGA curve (a) and its differential curve (b) for OMS-1-R24.

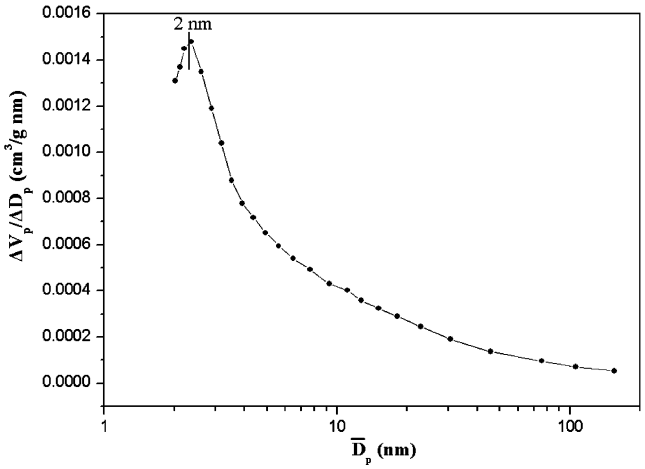

Figure 8. PVD curve of OMS-1-R24 constructed by BHJ analysis.

tunnel structure of OMS-1-R24 and its thermal stability. Removal of tunnel water below 400 °C led to an increase in void space for N_2 accommodation. A decrease in surface area with the calcined temperature then indicated partial or complete collapse of the tunnel structure.

The TGA curve and its differential curve for OMS-1-R24 showed five weight loss steps at temperature ranges of 50−105, 105−240, 240−405, 405−580, and 580−700 °C, respectively (Figure 7). Similar to natural todorokite, OMS-1-R24 remained a todorokite structure below 400 °C.[30,31] Weight loss below 105 °C was probably due to the loss of water physically adsorbed on the surface. As the temperature increased, Mn was reduced and O was released, and then the octahedral framework started to break down and loss of the water bound in the tunnel occurred.[31] The last two steps of weight loss could be attributed to the great destruction and collapse of tunnel structure, respectively.[29,30] Consequently, OMS-1-R could keep thermally stable up to 400 °C and was not quite as stable as hydrothermally synthesized OMS-1 reported by Suib and co-workers.[4,29]

Surface Area, Porosity, and Chemical Compositions. The specific surface area of OMS-1-R24 derived from BET analysis was 77 m^2/g. The nitrogen adsorption−desorption isotherm determined on OMS-1-R24 was type-IV, implying that its surface was predominantly mesoporous[18] (see Supporting Information). The average pore diameter was 14 nm as determined by BHJ cumulative calculations. A BHJ analysis of the adsorption data resulted in the pore volume distribution (PVD) curve given in Figure 8. Pores of a mean diameter at ≤2 nm are micropores.[32,33] The PVD curve displayed a peak at 2 nm, indicating the presence of narrower pores. The micropore volume determined from the *t*-plot[32] was 0.0018 cm^3/g, only 1% of the total pore volume (0.17 cm^3/g) derived from the adsorption isotherm. Thus, the pore structure of OMS-1-R24 mainly consisted of mesopores, and the micropores were in the minority, which was similar to the hydrothermally synthesized todorokite.[33] We observed no peak within the mesoporous range of the PVD curve, perhaps due to the scattering of the mesopore distribution on the surface of OMS-1-R24. The chemical compositions of OMS-1-R8 and OMS-1-R24 were $Mg_{0.19}MnO_{2.11}(H_2O)_{1.15}$ and $Mg_{0.17}MnO_{2.10}(H_2O)_{0.88}$, respectively. These stoichiometries resembled those of hydrothermally synthesized todorokites reported in the literature, except for those with a higher AOS[6,11,24] or a lower content of Mg relative to those of OMS-1 synthesized by Suib and co-workers.[4,29]

In this study, birnessite was prepared with a modified method in which highly vigorous stirring was used to increase the fluxion velocity of the reaction suspension. A more effective oxidation process occurred during the synthesis, and a high AOS of Mn was obtained for this mineral.[15] Thus, the Mn^{3+} substitutions for Mn^{4+} in the MnO_6 octahedral layer of birnessite were small in quantity, while the repulsion between MnO_6 octahedron was more effective, facilitating the transfer of Mn in the MnO_6 octahedral layer to the interlayer to construct a tunnel structure. This was probably one of the reasons why todorokite could be successfully synthesized under the mild condition of refluxing.

Conclusions

Thermally stable and well-crystallined todorokites were synthesized by a heating and refluxing process using birnessite as a precursor. The average chemical composition of the synthesized todorokites by refluxing for 8 and 24 h was $Mg_{0.19}MnO_{2.11}(H_2O)_{1.15}$ and $Mg_{0.17}MnO_{2.10}(H_2O)_{0.88}$, respectively. The crystallinity of the todorokite was promoted with the increased reflux time, and no other phase was produced. The synthesized todorokites exhibited the same morphologies and structural characteristics similar to those of both the natural todorokites and the hydrothermally synthesized samples. The pore structure of OMS-1-R mainly consisted of mesopores. The chemical compositions of the synthetic tordorokites by the refluxing process were close to those of todorokites synthesized by a hydrothermal process, except for a higher average oxidation state of Mn of todorokites synthesized in this study.

(30) Bish, D. L.; Post, J. E. *Am. Mineral.* **1989**, *74*, 177−186.
(31) Post, J. E.; Heaney, P. J.; Hanson, J. *Am. Mineral.* **2003**, *88*, 142−150.
(32) Gregg, S. J. In *Adsorption at the Gas−Solid and Liquid−Solid Interface*; Rouquerol, J., Sing, K. S. W., Eds.; Elsevier: Amsterdam, 1982; pp 153−164.
(33) Ali, A. A.; Al-Sagheer, F. A.; Zaki, M. I. *Int. J. Inorg. Mater.* **2001**, *3*, 427−435.

Acknowledgment. We gratefully acknowledge the reviewers for their helpful comments. We are thankful to Dr. J. Z. He and Dr. S. Tu for reviewing the final draft, to Dr. X. W. Liu for his assistance with TEM analysis, to Ms. L. Huang for her help with the ASAP 2020 instrument, and to Dr. M. C. He for help in Raman analysis. We also thank the National Natural Science Foundation of China for financial support of this research (Grant Nos. 40101017 and 40071048).

Supporting Information Available: Synthetic details, TEM images, Raman spectra, and a nitrogen adsorption−desorption isotherm (PDF). This material is available free of charge via the Internet at http://pubs.acs.org.

CM0499545